Spontaneous and Ion-Specific Formation of Inverted Bilayers at Air/Aqueous Interface

Srikanth Nayak, Raju R. Kumal, and Ahmet Uysal[*]

Chemical Sciences and Engineering Division, Argonne National Laboratory, Lemont, IL 60439

KEYWORDS

Liquid-liquid extraction, Langmuir monolayers, inverted bilayers, lanthanide separation, ion-specific effects, amphiphile aggregation, vibrational sum frequency generation, ion adsorption

ABSTRACT

Developing better separation technologies for rare earth metals is important for a sustainable economy. However, the chemical similarities between rare earths make their separations difficult. Identifying molecular scale interactions that amplify the subtle differences between the rare earths can be useful in developing new separation technologies. Here, we describe ion-dependent monolayer to inverted bilayer transformation of extractant molecules at the air/aqueous interface. The inverted bilayers form with Lu^{3+} ions but not with Nd^{3+}. By introducing Lu^{3+} ions to preformed monolayers, we extract kinetic parameters corresponding to the monolayer to inverted bilayer conversion. Temperature-dependent studies show Arrhenius behavior with an energy barrier of 40 kcal/mol. The kinetics of monolayer to inverted bilayer conversion is also affected by the character of the background anion, although anions are expected to be repelled from the interface. Our results show the outsized importance of ion-specific effects on interfacial structure and kinetics, pointing to their role in chemical separation methods.

INTRODUCTION

Liquid-liquid extraction (LLE) is a chemical separation process widely used in hydrometallurgical processing of minerals, nuclear waste, and in recycling.[1] Despite being used for decades, molecular-scale details of LLE are not well-understood. A clear identification of free energy drivers in LLE will lead to more efficient separation technologies, a crucial task due to the increasing demand for rare earths (REs), platinum group metals, and other critical materials.

LLE is a two-phase free-energy driven process, involving complex ionic equilibria in both phases, interfacial effects, and solvent reorganization.[2] The selective interfacial transport of metallic ions is thought to be mainly driven by the amphiphilic extractant molecules used in LLE.[3] Thus, model systems focusing on the interfacial interactions of ions with amphiphilic molecules have been used to elucidate the processes in LLE.[4]

Dialkyl phosphoric acid extractants have been widely used in LLE of metals, particularly RE elements.[5] Bis(2-ethylhexyl) phosphoric acid (HDEHP) preferentially extracts the heavier lanthanides in a dimeric form such that there are six phosphate groups coordinating the extracted lanthanide in the organic phase.[6] Reverse micellar structures are formed in the organic phase after extraction of metals with HDEHP.[7] Interfacial studies using vibrational sum-frequency generation (VSFG) spectroscopy have shown the importance of hydrogen bonding interactions between the phosphate groups and water in stabilizing these micellar structures at the liquid-liquid interface.[8] Peak shifts in VSFG in the phosphate region induced by different lanthanides have been attributed to increasing interaction strength between HDEHP and the lanthanides with increasing atomic number.[9] Interestingly, interfacial X-ray scattering and fluorescence results suggest a preference for lighter lanthanides at the Gibbs monolayers of HDEHP at the air/aqueous interface, due to the higher solubility of HDEHP complexes of heavier lanthanides.[10]

Water-insoluble molecules, with longer alkyl tails, are limited to interface and can plausibly provide more information on the ion-extractant interactions. Dihexadecylphosphate (DHDP) forms an insoluble monolayer on water, and it has been used as an analogue of HDEHP for this purpose.[4b, 4j, 11] At the dodecane-water interface, "kinetically arrested" inverted bilayer of DHDP-Er(III) complexes has been observed.[4c, 11] This phenomena was proposed to underlie the micellization in the organic phases after LLE.[4c] Extraction of divalent and trivalent ions were compared.[4c]

Langmuir monolayers at air-water interface are convenient model systems for LLE and have been well studied to probe intermolecular forces.[4a, 12] Influence of dissolved chemical species on monolayers has been studied in order to understand the intermolecular interactions in various biological and physicochemical systems.[13] Changes in the physical state of the interface are typically monitored by surface pressure isotherms, X-ray and neutron scattering techniques, vibrational spectroscopy, and light microscopy techniques.[12, 13d, 14] However, majority of the studies have been under static conditions, a drawback in understanding kinetics of extractant ion interactions in ion-transport.

Here, we show that the inverted bilayers of DHDP can be created at air/aqueous interface, allowing kinetic and temperature-dependent studies. Using synchrotron X-ray scattering techniques and VSFG, we first show that the inverted bilayers form with Lu^{3+} but not with Nd^{3+}, chemically very similar lanthanides, which shows that the charge density of the metal ion is the main driver behind the inverted bilayer formation. Bilayers can form regardless of the monolayer spreading procedure: a) when DHDP is spread on Lu^{3+} containing solutions, inverted bilayers form immediately, b) when DHDP monolayer is spread on pure water and Lu^{3+} ions are introduced later, the monolayer transforms into an inverted bilayer spontaneously. Temperature dependent studies

determined that the monolayer to inverted bilayer transition follows first order kinetics with an Arrhenius behavior. Very interestingly, background anions, such as nitrate and thiocyanate, significantly affect the bilayer formation kinetics, although they are expected to be repelled from the interface due to electrostatic interactions. We discuss the static monolayer and bilayer structures in detail and investigate the kinetics of bilayer formation with multiple probes.

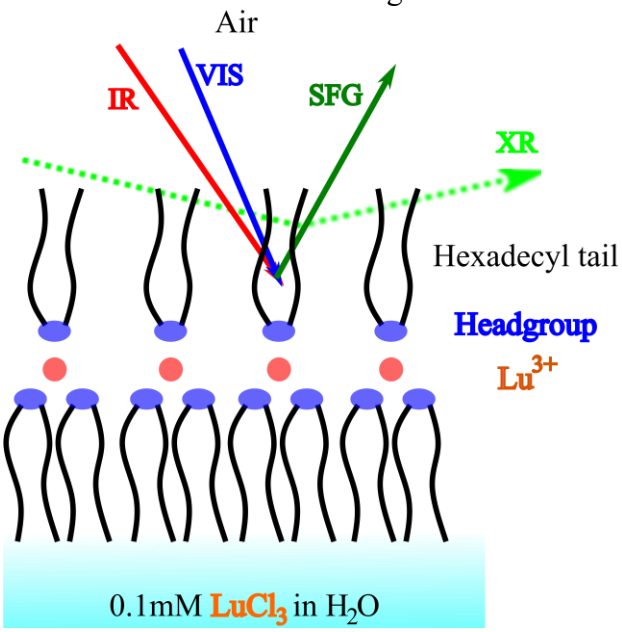

Figure 1. Schematic depiction of the experiments to probe interaction of DHDP molecules with Lu^{3+} ions at the air/aqueous interface. Samples are prepared by spreading DHDP on aqueous solutions of trivalent ions (See SI Methods). Specular XR and VSFG are complementary techniques that provide surface-specific structural information.

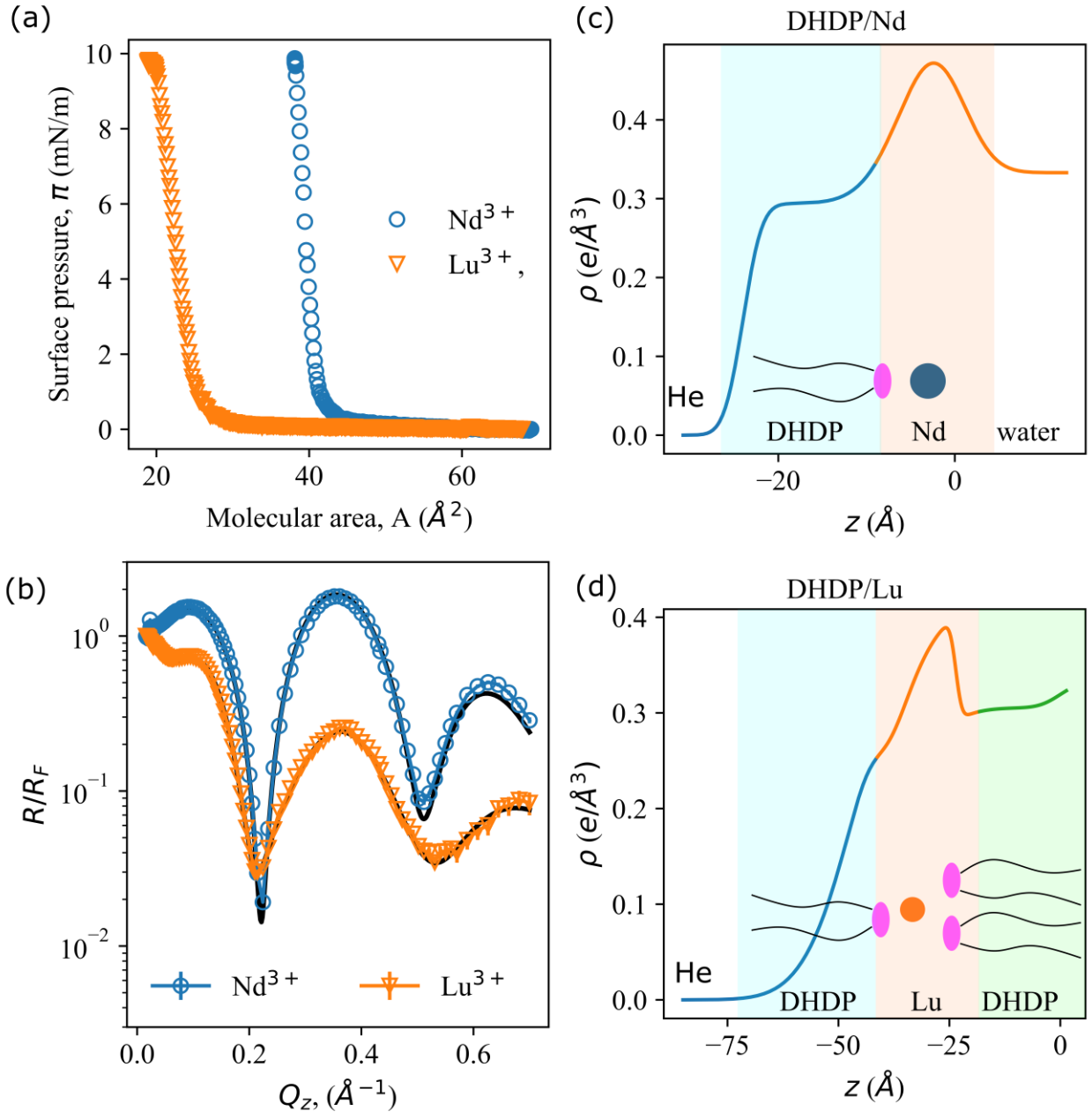

Figure 2. a) Langmuir isotherms showing the formation of monolayers of DHDP on surface of water (blue), 0.1 mM $SrCl_2$ (orange), 0.1 mM $NdCl_3$ (green), and inverted bilayer with 0.1 mM $LuCl_3$. b) X-ray reflectivity results for 0.1 mM $NdCl_3$ (blue circles) and 0.1 mM $LuCl_3$ in water (orange squares) and the corresponding EDPs in (c) and (d). The fits for $NdCl_3$ were obtained using a 2-box model corresponding to the monolayer tail region and the headgroup region. The fits for $LuCl_3$ were obtained with a 3-box model and it shows the formation of an inverted bilayer

at the air/aqueous interface. Schematics of the interfacial structure with Nd^{3+} and Lu^{3+} are also shown in (c) and (d).

Figure 2(a) shows the isotherms obtained by the compression of DHDP-covered surfaces, a common method to study Langmuir monolayers,[12] in the presence of either of the lanthanide ions. In the presence of Nd^{3+}, the surface pressure increases rapidly as the surface area is compressed to ~ 40 $Å^2$ per DHDP. This is typical for a monolayer of double-chain molecule, considering that the molecular area for a single hydrocarbon tail is ~ 20 $Å^2$. In contrast, in the presence of Lu^{3+} in the subphase, the surface pressure begins to rise at much lower values of surface area per DHDP. The lower area per DHDP (~ 27 $Å^2$) in the presence of Lu^{3+} suggests the formation of bilayer or multilayer at the surface.

The interfacial structure can be resolved by specular X-ray reflectivity (XR) as it provides information on the electron density profile (EDP) normal to the surface.[15] Figure 2(b) shows the Fresnel-normalized XR obtained for DHDP-covered surfaces in the presence of Nd^{3+} and Lu^{3+}. There are major qualitative differences in the reflectivity curves – with Nd^{3+} the normalized reflectivity rises at low Q_z whereas it decreases in the presence of Lu^{3+}. Further, the first extremum occurs at a smaller Q_z for Lu^{3+} surfaces. EDPs obtained from the box-model fits to the reflectivity curves are shown in Figure 2(c) and (d). The fit parameters are given in the Table S2 which provide information on the thickness of the layer (d), electron density (ρ), and roughness (σ). The interfacial region is wider in the case of Lu^{3+} compared to that of Nd^{3+}, which matches with the corresponding lower period of oscillations in the reflectivity curve. The EDP for Nd^{3+} sample precisely follows the expected profile for a monolayer, similar to those obtained with La^{3+}.[16] The boxes used in the fit correspond to the expected physical properties of the system – tail group region with a thickness of ~ 20 Å and electron density ~ 0.29 e/$Å^3$ corresponding to a closely packed alkyl chain region. The integrated electron density of the headgroup region is ~ 2.5 e/$Å^2$ which includes contributions from the phosphate groups, adsorbed Nd^{3+} and water molecules. In the case of Lu^{3+}, the EDP suggests an inverted bilayer structure. However, the boxes do not appear to have one-to-one correspondence with the ideal molecular structure, which is expected due to possible interdigitation in the bilayer structure and the roughness of the interface. So, we perform an analysis of the EDP as below.

We ascribe the peak in EDP (at z ~ -30 Å) to a layer of Lu^{3+} ions (Figure 2d, orange). For a regular bilayer, the electron density should uniformly decrease from this Lu^{3+} layer to the bulk aqueous region. The presence of a lower density region in the EDP between this Lu^{3+} layer and the aqueous bulk region (ρ ~ 0.33) suggests the presence of alkane chains, which in turn indicates that the surface is covered with an inverted bilayer. There can be two canonical conformations for the inverted bilayer – two DHDP molecules exposed to the air side and one towards the aqueous side, or vice versa. We can decompose the EDP shown in Figure 2(d) into three regions – top, middle, and bottom layers (Figure 2d, blue, orange, and green). We assume that the DHDP tail groups are fully extended in both top and bottom layers. This assumption is supported by the absence of any gauche defects (2850 cm^{-1} band) in the alkyl chains as shown by the VSFG spectra (Figure 3). Thus, we make the top and bottom layers to have approximately 20 Å thickness which corresponds to the full length of all-trans hexadecyl chains. This gives us an integrated electron density of ~ 2.6 e/$Å^2$, 7.5 e/$Å^2$, and 6.1 e/$Å^2$ for top, middle, and bottom layers, respectively. The higher electron density of the bottom layer than the top layer suggests that there are more DHDP molecules adjacent to the aqueous side. This conformation is favored possibly due to the higher

shielding of water from the chains with a tightly packed alkyl chain layer compared to a loosely packed alkyl chain region.

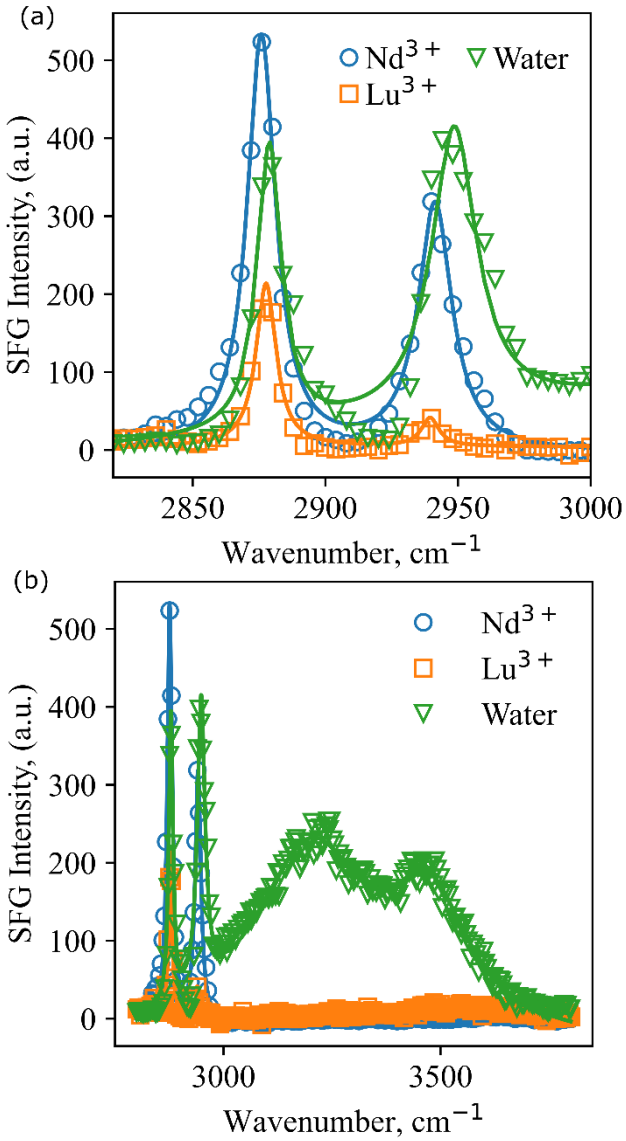

Figure 3. SFG spectra of DHDP/aqueous interface in the presence and absence of lanthanide ions showing (a) CH_2 and CH_3 stretch regions, and (b) OH stretch region. The concentration of lanthanide ions in the systems is 0.1mM each.

VSFG experiments proved further confirmation for the suggested bilayer structure. VSFG spectrum of the DHDP-Lu^{3+} system shows a decrease in CH_3 stretch peak intensity compared to DHDP-water case indicating lower asymmetry relative to a monolayer (Figure 3(a)). Since VSFG is a dipole forbidden process, molecules orienting opposite to each other either cancel or reduce the net dipole and lower the intensity. If the bilayer were symmetrical having equal number of the DHDP molecules on top and bottom, the overall peak intensity would reduce to zero. Thus, our VSFG result support the XR results showing unequal distribution of DHDP between top and bottom layers. In the presence of Nd^{3+} ions there is no decrease in intensity confirming the

monolayer structure. In fact, the signal slightly increases due to the better packing of the molecules as the headgroup charge is shielded by the adsorbed ions, reducing the repulsion. The corresponding spectra in the OH region provides the interfacial water structure (Figure 3(b)).)). On pure water, the electric field of the headgroups orient the water molecules inducing a strong signal. In the case of Nd^{3+}, ions shield the charge of the headgroup diminishing the VSFG signal. [4d, 17] In the case of Lu^{3+}, inverted bilayer forms and the tails touching the surface do not create any significant orientational ordering.[4d, 17]

We can directly detect the metal ions in monolayer and inverted bilayer structures by X-ray fluorescence near total reflection (XFNTR) spectroscopy.. Figure S4 shows the variation of integrated fluorescence signal in the L_α region of Nd and Lu as a function of the vertical momentum transfer (Q_z). The fits to the data provide an estimate of the interfacial number density of the elements (Table S1). For Nd^{3+} we obtain an area of ~ 116±4 $Å^2$ per Nd. At ~40 $Å^2$ per DHDP molecule there is ~ 0.34±0.01 Nd^{3+} per DHDP which is close to the Nd^{3+} number density required for balancing the charge of the monolayer. With Lu^{3+} however, we obtain 41±1$Å^2$ per Lu, or approximately 0.66 Lu per DHDP molecule at 27 $Å^2$ per DHDP. Assuming that the charge balance is satisfied only by DHDP and Lu^{3+} ions, the minimum surface area per Lu^{3+} when both the top and bottom DHDP layers are fully packed should be 120 $Å^2$ / 2 = 60 $Å^2$. As the obtained surface area is significantly less than this minimum, the speciation of Lu is probably different from the trivalent species found in bulk solution, i.e. counterions may be present in the bilayer to compensate the charge. Presence of divalent hydroxyl-lanthanide species next to an anionic monolayer have been recently reported.[18]

In the absence of any Lu^{3+} ions, DHDP forms a monolayer on water and this provides an opportunity to study the kinetics of the bilayer formation. XR of the interface after compressing DHDP on water to a surface pressure of 10 mN/m shows the formation of a monolayer (Figure 4, blue). Upon introduction of Lu^{3+} ions in the subphase, behind the trough barrier, the X-ray reflectivity shows a gradual change along with decrease in surface area for maintaining constant surface pressure. About 4.5 hours after the introduction of Lu^{3+}, the XR curve becomes very similar to the one shown in Figure 2(b) indicating that the interface has an inverted-bilayer structure similar to the one obtained by direct spreading of DHDP on Lu^{3+}-containing subphase (Figure 3, green).

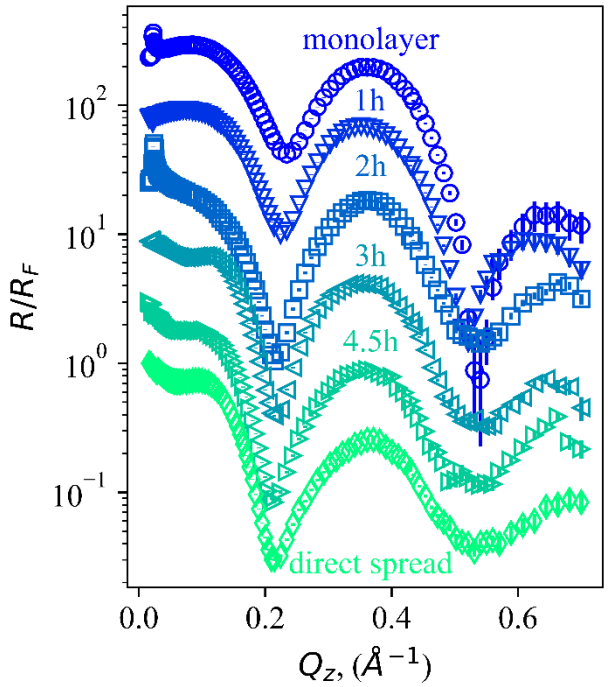

Figure 4. Time-dependent variation of the Fresnel-normalized XR profile of the DHDP-covered upon introduction of Lu^{3+} to the subphase. DHDP is spread on water and compressed to form a monolayer at a surface pressure of 10 mN/m. At t = 0, a small volume of $LuCl_3$ solution is injected into the subphase, behind the trough barrier. The monolayer begins to shrink in area while maintaining a constant surface pressure (see Figure 5(a) for the surface pressure isotherm). After ~4.5 hours, the XR profile of the surface resembles that of DHDP spread directly on $LuCl_3$ solution (Figure 2(b)). The XR curves at different time stamps have been shifted vertically for clarity.

The effect of monovalent anions on the interfacial adsorption and transport of lanthanides has been reported earlier.[4d, 4e, 19] We found no effect of background ions on the final static structure when spreading DHDP on the subphase containing lanthanides and background salts (Figure S5). However, there is an anion-dependence in the kinetics of monolayer to inverted bilayer transition (Figure 5) upon addition of Lu^{3+}. We spread DHDP monolayer on salt solutions (0.1 M of $NaNO_3$ or NaSCN) and introduced either Nd^{3+} or Lu^{3+} solution behind the barrier (Figure S2). The barrier position was allowed to move to maintain a constant surface pressure of 10 mN/m, same as the one used above. With introduction of Nd^{3+} the surface area remains constant with time (Figure S5). Figure 5(a) shows the decay of trough area required to maintain the surface pressure constant upon injecting Lu^{3+} solution. We have modeled the decay as an exponential function of time according to Equation S1. This model has three parameters - t_0 (time offset after which the decay is exponential), k (rate constant for exponential decay), and a_∞ (the ratio of final to initial trough area). The fit parameters are listed in Table S3. The rate of decay roughly corresponds to the monolayer to inverted bilayer transition. Thus, there is an effect of background anion on the monolayer to inverted bilayer transition. Both nitrate and thiocyanate increase the rate of transition with thiocyanate having a stronger effect.

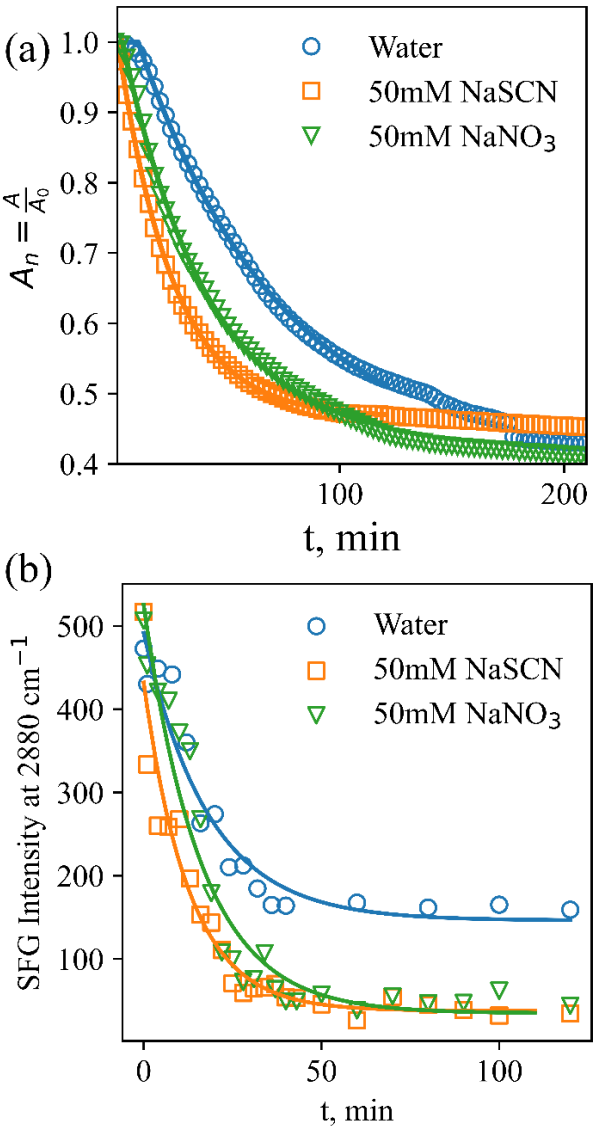

Figure 5. (a) The kinetics of the formation of the bilayer are dependent on the background anion present in the aqueous subphase. Thiocyanate (orange squares) leads to a faster formation of the bilayer compared to nitrate (green triangles), both faster than having no background salt (blue circles). The solid lines are fits to an empirical model based on nucleation growth theory shown in Eq. 1. (b) Decay rates of the amplitude of the CH_3 symmetric stretch peak from VSFG experiments also indicate that the monolayer to inverted bilayer transition is faster in the presence of NaSCN.

The intensity of CH_3 symmetric stretch peak in VSFG spectra, at 2875 cm^{-1}, provides a molecular scale description of monolayer to bilayer transition (Figure S3 and S6). Figure 5b shows the decay of this peak upon introduction of Lu^{3+} to the subphases below DHDP monolayers. An exponential decay model was used to fit the data (solid lines in Figure 5(b)) and the parameters are listed in Table S4. The rate of monolayer to inverted bilayer conversion is increased by background ions; and thiocyanate has a stronger effect than nitrate. The rate of conversion obtained from VSFG appears to be faster than corresponding rates obtained by surface pressure isotherms.

There may be a few reasons for the difference. First, VSFG probes the molecular scale structure directly, as opposed to the macroscopic surface area measurement. Also, a constant area setup used in VSFG versus the constant pressure setup in the isotherms can contribute to the differences (Figure S2). We note that the intensity of CH_3 symmetric stretch peak does not significantly change We investigated the temperature dependence of monolayer to bilayer transition to understand the energetics of the process (Figure 6a). The rate constant is derived from the fits to an empirical model based on the classical nucleation growth theory (Equation S1). Its variation as a function of the inverse temperature is shown in Figure 6b. The fit parameters are tabulated in Table S3. The linear relationship shows that the monolayer to inverted bilayer transition follows the Arrhenius equation. We obtain an activation energy of ~ 40 kcal/mol for the transition. Induction time for monolayer to inverted bilayer transition (t_0) decreases with increasing temperature.

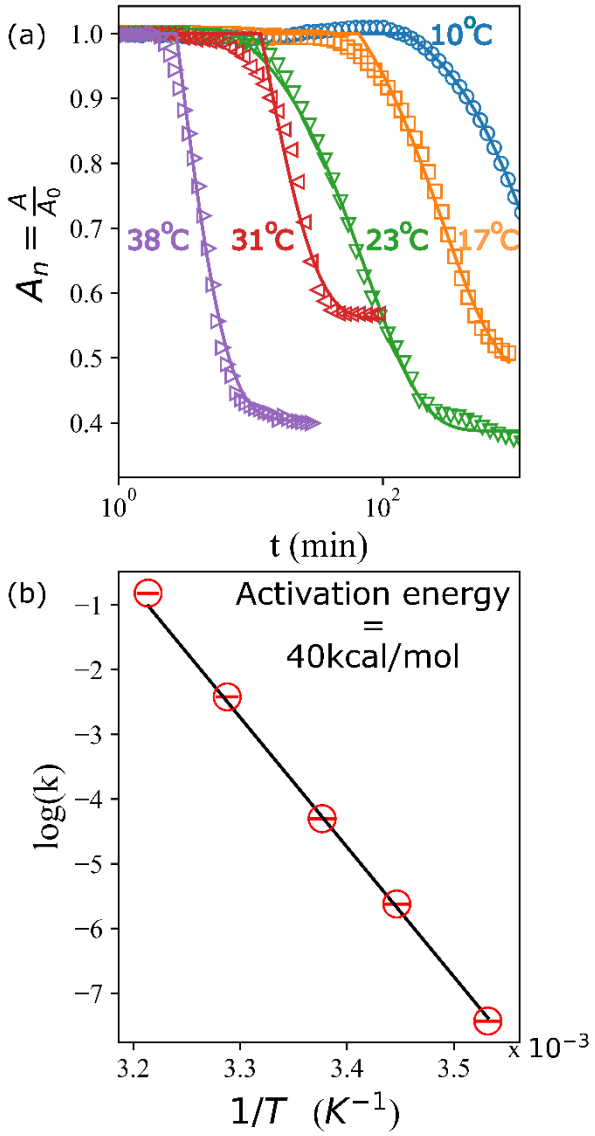

Figure 6. (a)Temperature dependence of the normalized area that is required to maintain a constant surface pressure of 10 mN/m as a function of time with injection of $LuCl_3$ to the subphase (final

concentration of 0.1mM). While at a low temperature of 10 ºC, the compression of surface due to the formation of the bilayer occurs in the scale of hours, at 38 ºC the transition occurs within minutes. Black solid lines show the fits obtained using an exponential decay, corresponding to first order kinetics of the transition (Eq. S1). (b) Variation of the first order rate constant (k) of monolayer–bilayer transition shows a classical Arrhenius type of behavior.

DISCUSSIONS

We have studied the differences in Lu^{3+} and Nd^{3+} adsorption onto DHDP-laden aqueous surfaces using X-ray scattering, VSFG, and surface pressure isotherms. We find that, regardless of the surface preparation method, DHDP forms an inverted bilayer structure in the presence of Lu^{3+} ions and a monolayer in the presence of Nd^{3+} ions (Figure 7). The qualitative difference between the nanoscale structures induced by different charge densities of Nd^{3+} and Lu^{3+} directly affects the macroscopic system, a desired property of chemical separation systems.

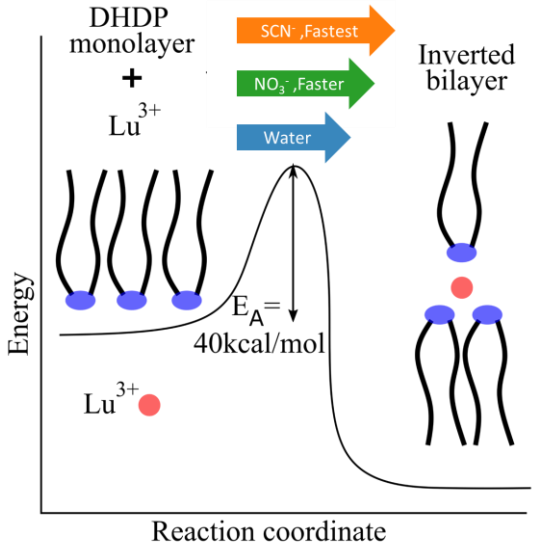

Figure 7. Schematic description of the monolayer to inverted bilayer transition of DHDP in the presence of Lu^{3+} ions based on Figures 5 and 6. The reaction follows first order kinetics with an energy barrier of 40 kcal/mol and is catalysed by background anions – SCN^- and NO_3^-.

Interfacial adsorption and transport of lanthanide ions is of great research interest due to their relevance in RE element separations.[1, 3] The effects of direct electrostatic interactions at the interface have been investigated.[4a, 4i] In the context of LLE, ion-surfactant interactions at the air/aqueous interface can elucidate both the dynamic ion transport across the interface and the equilibrium structures formed by the ion-extractant complexes in the organic phase. Dynamic structures forming at the liquid-liquid interface, such as water fingers, water ridges, and chemical "hinges" have been reported as some of the driving mechanisms for interfacial transport.[20] Self-assembly of extractant-ion aggregates at the interface can also play a dynamic role in the interfacial ion transport.[8] The ion-specific formation of inverted bilayer with Lu^{3+} indicates a possible difference in dynamics of ion transfer with lighter and heavier lanthanides even at longer time scales than that were investigated by simulations.

All the RE ions are predominantly +3 charged and the main difference between them is in their decreasing ionic sizes with increasing atomic number, a phenomenon known as the lanthanide contraction.[21] The chemistry of REs are dominated by electrostatic interactions in their crystalline compounds.[22] The mean-field theories developed for monovalent ions at dilute concentrations[23] usually fail to describe experimental observations with multivalent ions. Multivalent ions can induce "charge-reversal" or spontaneous collapse of monolayers which have not been reported with monovalent ions.[24] In this context, effects of ion-ion and ion-lipid correlations have been described.[4a, 25] Further, specific ion-lipid interactions such as hydrogen bonding and coordination bonds can lead to ion-specific interactions at the interface.[16, 26] Our results add a new dimension to these observations and show that the complex interactions of the trivalent ions can be fine-tuned to create qualitative differences in their interactions with amphiphiles, which directly affects the macroscopic behavior of the system.

We note that DHDP is used as an interfacial analogue to HDEHP in our study. It is important to consider the effects of tail structure. In LLE, the tail group plays a major role in extraction, organic phase structure and the phase behavior.[27] Similarly, the tail structure plays a major role in the formation and structure of the Langmuir monolayers due to the Van der Waals interactions between the tails.[12, 28]

Our results with DHDP at air-water interface and the prior results obtained with DHDP at water-dodecane interface show that an inverted bilayer of DHDP is formed with heavy, charge dense trivalent ions.[4c, 11] At the dodecane-water interface, Sr^{2+} adsorbs to a monolayer of DHDP at the interface.[4b] This difference between trivalent and divalent ions was interpreted as different extraction mechanisms for them with dialkyl phosphoric acid extractants.[4c] Here, we show that it is not necessarily a difference between divalent and trivalent ions, as Nd^{3+} behaves like Sr^{2+} as far as the formation of DHDP monolayers is concerned.

The dodecane-water interface experiments required lower temperatures to kinetically arrest the interfacial species formed during ion transfer. In contrast to the results obtained with DHDP, VSFG studies with HDEHP at the air-water interface suggest that HDEHP interacts with all the lanthanides in a monolayer-like structure.[9, 29] Similarly, XR of the HDEHP at the air-water interface is not qualitatively different for light and heavy lanthanides.[10] With a shorter chain analogue of HDEHP, namely dibutyl phosphate, a structure similar to inverted-bilayer is observed.[29] Organic phase speciation of Er is also different when extracted with HDEHP (hexamer) or DHDP (trimer).[11] Regardless of these differences, it is evident that the small changes in ionic size of the lanthanides can have a major implications to the organic phase structure and thereby the extraction energetics.

Although there are several studies on the collapse of Langmuir monolayers due to compression[30] there are fewer on the spontaneous collapse of monolayers induced by solutes. Recently, a spontaneous monolayer to inverted bilayer transformation of palmitic acid in the presence of calcium ions has been reported.[24b] Divalent cations have also been shown to reduce the surface pressure at which stearic acid films collapse.[31] Such interplay of ion-lipid interactions is especially important in the biophysics of cellular membranes where lipids affect selective ion transport and ions affect transbilayer lipid motions.[32] In this context, , a coordination-driven, ion-specific monolayer to inverted bilayer transition has been reported with calix[4]arene films on Cu(II) or Ni(II) solutions.[33] Unlike the lanthanide ions where ligands interact electrostatically, transition metals can show significant selectivities due to ligand-metal coordination bonds that are directional.

The kinetics of monolayer to inverted bilayer transition with Lu^{3+} in the subphase is strongly temperature dependent with an activation barrier of ~ 40kcal/mol. This relatively large energy barrier is in correspondence with the lower temperature required to arrest the heavy lanthanide species at the dodecane-water interface.[11] The onset of transition is also temperature dependent indicating a temperature dependent nucleation of inverted bilayer structure. DHDP forms stable monolayers with Nd^{3+} in the subphase at temperatures up to 37 ºC. Whether inverted bilayers can form with lighter lanthanides at higher temperatures is an open question. It is not clear whether inverted bilayer formation is kinetically limited or the inverted bilayers are thermodynamically unstable with Nd^{3+}.

We have previously reported the anion-dependence in lanthanide adsorption at DHDP monolayers.[4e] These experiments were conducted with preformed monolayers and lanthanide injection behind the barrier. Under the impression that the surfaces were under equilibrium, we attributed the differences in fluorescence signals to anion-effect on number density of lanthanides adsorbing to the surface. We obtained an interfacial area per Lu that is lower than that for 1:3 Lu:DHDP complexes and interpreted that to be a result of excess background anions. Our current work shows that the lower interfacial area per Lu is obtained even in the absence of excess background salts. Further, the reported difference in Lu adsorption with different background salts are due to the differences in kinetics of inverted bilayer formation in the presence of NO_3^- and SCN^-.

CONCLUSIONS

We have demonstrated how monolayer to bilayer conversion can be used to identify important ion-specific effects in RE separations. Phosphoric acid based extractants are often used in the LLE of RE elements, but there are outstanding questions on the mechanisms that determine ion transport and selectivity. Here we have shown that there is an ion-specific effect in the adsorption of trivalent ions to DHDP, an analogue of phosphoric acid based extractants: larger trivalent ion Nd^{3+} maintains the monolayer structure of DHDP while smaller Lu^{3+} ion induces the formation of an inverted bilayer. This shows that the air/aqueous interface models can be used to reproduce important aspects of oil/water interfaces. Further, the monolayer of DHDP collapses to an inverted bilayer upon the introduction of Lu^{3+} ions where the rate of collapse is temperature dependent. These results show that the minor differences in ionic sizes of the RE elements have major impacts on the interfacial structure. Elucidating these effects at the air-water interface, can show the drivers of ion-transport and selectivity in LLE. The kinetics of ion-dependent monolayer to inverted bilayer transition provide a route to investigate ion transport and lipid structure in various physicochemical processes.

AUTHOR INFORMATION

Corresponding Author

*Email: ahmet@anl.gov. Web: www.anl.gov/profile/ahmet-uysal

Author Contributions

The manuscript was written through contributions of all authors. All authors have given approval to the final version of the manuscript.

Notes

Authors declare no competing financial interest.

ACKNOWLEDGEMENTS

We thank Wei Bu for his help with the liquid surface synchrotron experiments. The work presented here is supported by the U.S. Department of Energy, Office of Basic Energy Science, Division of Chemical Sciences, Geosciences, and Biosciences, Separation Science program under contract DE-AC02-06CH11357. Use of the Advanced Photon Source, an Office of Science User Facility operated for the U.S. Department of Energy (DOE) Office of Science by Argonne National Laboratory, was supported by the U.S. DOE under Contract No. DE-AC02-06CH11357. NSF's ChemMatCARS Sector 15 is principally supported by the Divisions of Chemistry (CHE) and Materials Research (DMR), National Science Foundation, under Grant NSF/CHE-1834750.

ABBREVIATIONS

XFNTR, X-ray fluorescence near total reflection; VSFG, vibrational sum frequency generation; LLE, liquid-liquid extraction; XR, X-ray reflectivity; DHDP, Dihexadecylphosphate;

ASSOCIATED CONTENT

SUPPORTING INFORMATION.

The supporting information document has the following: a) VSFG spectra showing the OH region, b) results from X-ray fluorescence near total reflection, c) X-ray reflectivity curves in the presence of salts, d) Surface pressure isotherm of DHDP on Nd^{3+} solution showing its stability, and e) Fit parameters for the empirical model describing the kinetics of monolayer to inverted bilayer transition.

REFERENCES

[1] B. Moyer, in *Ion Exchange and Solvent Extraction, Vol. 23*, 1st ed., CRC Press, Boca Raton, **2020**, p. 310.

[2] a) A. M. Wilson, P. J. Bailey, P. A. Tasker, J. R. Turkington, R. A. Grant, J. B. Love, *Chem. Soc. Rev.* **2014**, *43*, 123-134; b) J. J. M. Nelson, E. J. Schelter, *Inorg. Chem.* **2019**, *58*, 979-990.

[3] A. E. Clark, *ACS Cent. Sci.* **2019**, *5*, 10-12.

[4] a) M. Miller, Y. Liang, H. Li, M. Chu, S. Yoo, W. Bu, M. Olvera de la Cruz, P. Dutta, *Phys. Rev. Lett.* **2019**, *122*, 058001; b) W. Bu, M. Mihaylov, D. Amoanu, B. H. Lin, M. Meron, I. Kuzmenko, L. Soderholm, M. L. Schlossman, *J. Phys. Chem. B* **2014**, *118*, 12486-12500; c) Z. Liang, W. Bu, K. J.

Schweighofer, D. J. Walwark, J. S. Harvey, G. R. Hanlon, D. Amoanu, C. Erol, I. Benjamin, M. L. Schlossman, *Proc. Natl. Acad. Sci. U.S.A* **2019**, *116*, 18227-18232; d) K. Lovering, S. Nayak, W. Bu, A. Uysal, *J. Phys. Chem. C* **2020**, *124*, 573-581; e) S. Nayak, K. Lovering, W. Bu, A. Uysal, *J. Phys. Chem. Lett.* **2020**, *11*, 4436-4442; f) S. Nayak, R. R. Kumal, Z. Liu, B. Qiao, A. E. Clark, A. Uysal, *ACS Appl. Mater. Interfaces* **2021**, *13*, 24194-24206; g) W. Rock, B. F. Qiao, T. C. Zhou, A. E. Clark, A. Uysal, *J. Phys. Chem. C* **2018**, *122*, 29228-29236; h) A. Uysal, W. Rock, B. F. Qiao, W. Bu, B. H. Lin, *J. Phys. Chem. C* **2017**, *121*, 25377-25383; i) E. Scoppola, E. B. Watkins, R. A. Campbell, O. Konovalov, L. Girard, J. F. Dufreche, G. Ferru, G. Fragneto, O. Diat, *Angew. Chem., Int. Ed.* **2016**, *55*, 9326-9330; j) N. F. Zhou, R. D. Neuman, *Colloids Surf.* **1992**, *63*, 201-207.

[5] D. Q. Li, *J. Rare Earths* **2019**, *37*, 468-486.

[6] K. L. Nash, *Solvent Extr. Ion. Exc.* **2015**, *33*, 1-55.

[7] a) R. D. Neuman, N. F. Zhou, J. G. Wu, M. A. Jones, A. G. Gaonkar, S. J. Park, M. L. Agrawal, *Sep. Sci. Technol.* **1990**, *25*, 1655-1674; b) T. H. Ibrahim, *Sep. Sci. Technol.* **2011**, *46*, 2157-2166; c) D. C. Steytler, T. R. Jenta, B. H. Robinson, J. Eastoe, R. K. Heenan, *Langmuir* **1996**, *12*, 1483-1489; d) T. S. Grimes, M. P. Jensen, L. Debeer-Schmidt, K. Littrell, K. L. Nash, *J. Phys. Chem. B* **2012**, *116*, 13722-13730.

[8] A. U. Chowdhury, L. Lin, B. Doughty, *ACS Appl. Mater. Interfaces* **2020**, *12*, 32119-32130.

[9] R. Kusaka, M. Watanabe, *J. Phys. Chem. B* **2021**, *125*, 6727-6731.

[10] P. Sun, E. A. Binter, Z. Liang, M. A. Brown, A. V. Gelis, I. Benjamin, M. K. Bera, B. Lin, W. Bu, M. L. Schlossman, in *ChemRxiv*, **2021**.

[11] W. Bu, H. Yu, G. Luo, M. K. Bera, B. Hou, A. W. Schuman, B. Lin, M. Meron, I. Kuzmenko, M. R. Antonio, L. Soderholm, M. L. Schlossman, *J. Phys. Chem. B* **2014**, *118*, 10662-10674.

[12] V. M. Kaganer, H. Mohwald, P. Dutta, *Rev. Mod. Phys.* **1999**, *71*, 779-819.

[13] a) M. Elderdfi, A. F. Sikorski, *Chem. Phys. Lipids* **2018**, *212*, 61-72; b) M. Ahlers, W. Muller, A. Reichert, H. Ringsdorf, J. Venzmer, *Angew. Chem., Int. Ed.* **1990**, *29*, 1269-1285; c) P. Dynarowicz-Latka, A. Dhanabalan, O. N. Oliveira, Jr., *Adv. Colloid Interface Sci.* **2001**, *91*, 221-293; d) J. J. Giner-Casares, G. Brezesinski, H. Mohwald, *Curr. Opin. Colloid. Interface Sci.* **2014**, *19*, 176-182; e) J. B. Li, Z. J. Chen, X. L. Wang, G. Brezesinski, H. Mohwald, *Angew. Chem., Int. Ed.* **2000**, *39*, 3059-3062.

[14] a) C. Stefaniu, G. Brezesinski, *Curr. Opin. Colloid. Interface Sci.* **2014**, *19*, 216-227; b) W. Sung, D. Kim, Y. R. Shen, *Curr. Appl. Phys.* **2013**, *13*, 619-632; c) D. Vollhardt, *Curr. Opin. Colloid. Interface Sci.* **2014**, *19*, 183-197.

[15] a) M. K. Bera, W. Bu, A. Uysal, in *Physical Chemistry of Gas-Liquid Interfaces*, Elsevier, **2018**, pp. 167-194; b) P. S. Pershan, M. Schlossman, *Liquid surfaces and interfaces: synchrotron x-ray methods*, Cambridge University Press, **2012**.

[16] W. Wang, R. Y. Park, D. H. Meyer, A. Travesset, D. Vaknin, *Langmuir* **2011**, *27*, 11917-11924.

[17] R. Kumal, S. Nayak, W. Bu, A. Uysal, in *ChemRxiv*, ChemRxiv, **2021**.

[18] S. Adrien, S. Sanghamitra, A. Ellen, C. Robert, A. Heather, T. Eric, in *ChemRxiv*, ChemRxiv, **2021**.

[19] S. Nayak, K. Lovering, A. Uysal, *Nanoscale* **2020**, *12*, 20202-20210.

[20] a) N. Kikkawa, L. Wang, A. Morita, *J. Am. Chem. Soc.* **2015**, *137*, 8022-8025; b) B. Wen, C. Sun, W. Zheng, B. Bai, E. Lichtfouse, *Soft Matter* **2020**, *16*, 826-832; c) B. Qiao, J. V. Muntean, M. Olvera de la Cruz, R. J. Ellis, *Langmuir* **2017**, *33*, 6135-6142; d) L. Benjamin, *Science* **1993**, *261*, 1558-1560; e) Z. Liu, A. E. Clark, *Chem. Sci.* **2020**, *12*, 2294-2303.

[21] a) S. A. Cotton, P. R. Raithby, *Coord. Chem. Rev.* **2017**, *340*, 220-231; b) M. Seitz, A. G. Oliver, K. N. Raymond, *J. Am. Chem. Soc.* **2007**, *129*, 11153-11160.

[22] a) R. E. Wilson, T. J. Carter, M. Autillo, S. Stegman, *Chem. Commun.* **2020**, *56*, 2622-2625; b) K. Dehnicke, A. Greiner, *Angew. Chem., Int. Ed.* **2003**, *42*, 1340-1354.

[23] a) P. Claesson, A. M. Carmonaribeiro, K. Kurihara, *J. Phys. Chem.* **1989**, *93*, 917-922; b) W. Bu, D. Vaknin, A. Travesset, *Langmuir* **2006**, *22*, 5673-5681; c) E. Leontidis, *Adv. Colloid Interface Sci.* **2017**, *243*, 8-22.
[24] a) M. Miller, M. Chu, B. Lin, M. Meron, P. Dutta, *Langmuir* **2016**, *32*, 73-77; b) P. Zhang, T. Pham, X. Zheng, C. Liu, P. L. Plata, P. Kral, W. Bu, B. Lin, Y. Liu, *Colloids Surf. B* **2020**, *193*, 111100.
[25] A. Travesset, D. Vaknin, *Europhys. Lett.* **2006**, *74*, 181-187.
[26] W. Sung, D. Vaknin, D. Kim, *J. Opt. Soc. Korea* **2013**, *17*, 10-15.
[27] a) M. J. Servis, D. T. Wu, J. C. Shafer, *J. Mol. Liq.* **2018**, *253*, 314-325; b) M. C. Dul, B. Braibant, S. Dourdain, S. Pellet-Rostaing, D. Bourgeois, D. Meyer, *J. Fluorine. Chem.* **2017**, *200*, 59-65; c) P. R. V. Rao, Z. Kolarik, *Solvent Extr. Ion. Exc.* **1996**, *14*, 955-993; d) Z. Kolarik, *Solvent Extr. Ion. Exc.* **2010**, *28*, 707-763.
[28] a) J. G. Petrov, T. Pfohl, H. Mohwald, *J. Phys. Chem. B* **1999**, *103*, 3417-3424; b) M. Y. Li, A. A. Acero, Z. Q. Huang, S. A. Rice, *Nature* **1994**, *367*, 151-153.
[29] R. Kusaka, M. Watanabe, *Phys. Chem. Chem. Phys.* **2018**, *20*, 2809-2813.
[30] a) M. D. Phan, J. Lee, K. Shin, *J. Oleo. Sci.* **2016**, *65*, 385-397; b) K. Y. Lee, *Annu. Rev. Phys. Chem.* **2008**, *59*, 771-791; c) W. Bu, D. Vaknin, *Langmuir* **2008**, *24*, 441-447; d) D. Vaknin, W. Bu, S. K. Satija, A. Travesset, *Langmuir* **2007**, *23*, 1888-1897.
[31] K. Das, B. K. Sah, S. Kundu, *Phys. Rev. E* **2017**, *95*, 022804.
[32] a) T. Heimburg, *Biophys. Chem.* **2010**, *150*, 2-22; b) L. Redondo-Morata, M. I. Giannotti, F. Sanz, *Mol. Membr. Biol.* **2014**, *31*, 17-28; c) K. Matsuzaki, S. Yoneyama, O. Murase, K. Miyajima, *Biochemistry* **1996**, *35*, 8450-8456; d) J. Lin, R. Dargazany, A. Alexander-Katz, *Small* **2017**, *13*; e) Y. H. Ma, B. L. Li, J. J. Yang, X. F. Han, Z. Chen, X. L. Lu, *J. Phys. Chem. C* **2019**, *123*, 17899-17907; f) S. Matile, K. Nakanishi, *Angew Chem Int Edit* **1996**, *35*, 757-759.
[33] M. Moradi, N. L. Lengweiler, C. E. Housecroft, L. G. Tulli, H. Stahlberg, T. A. Jung, P. Shahgaldian, *J. Phys. Chem. B* **2021**, *125*, 4204-4211.

TOC Figure

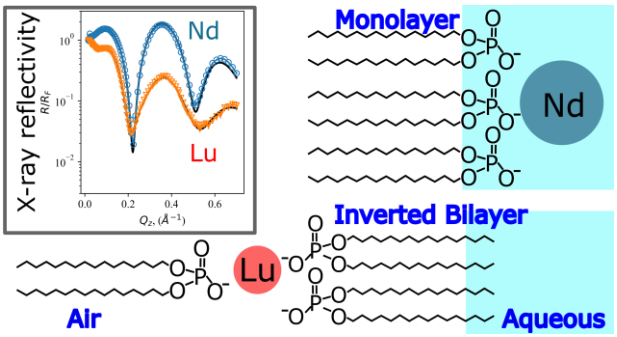
X-ray reflectivity
Nd
Lu
Monolayer
Nd
Inverted Bilayer
Lu
Air
Aqueous